JOURNAL OF GEOPHYSICAL RESEARCH, VOL. 114, A02217, doi:10.1029/2008JA013480, 2009

Storm-dependent radiation belt electron dynamics

Weichao Tu,[1] Xinlin Li,[1] Yue Chen,[2] G. D. Reeves,[2] and M. Temerin[3]

Received 12 June 2008; revised 22 October 2008; accepted 12 December 2008; published 28 February 2009.

[1] Using recently published electron phase space densities (PSD) as a function of L^* (L^* is approximately the radial distance in Earth radii at the equator) and time, energization and loss in the Earth's outer electron radiation belt were studied quantitatively and numerically using a radial diffusion model that included finite electron lifetimes and an internal source parameterized as a function of geomagnetic indices. We used PSD data at fixed values of the first and second adiabatic invariants, corresponding to electrons mirroring near the Earth's equator with an energy of ~2.7 MeV at $L^* = 4$. Model results for the second half of 2002 reproduced the average variations of the radiation belt electron PSD between $L^* = 2.5$ and $L^* = 6$ but with overprediction and underprediction at different times, implying that the same set of parameters cannot be applied to all storms. A detailed analysis of four individual storms showed that while electrons in three storms could be well simulated by energization from either radial diffusion only or internal heating only, incorporating both yielded the best results. For the other storm, an additional source of electrons was required to account for the enhanced PSD. The model results indicated that each storm is best simulated when a combination of radial diffusion and internal heating is used. Different storms required different magnitudes of radial diffusion and internal heating, and the relative contributions of these two acceleration mechanisms varied from storm to storm. A comparison of the results from different runs for the four storms and an analysis of the radial diffusion coefficients further suggest that internal heating contributes more to the enhancement of 2.7 MeV electrons at $L^* = 4$ than radial diffusion.

Citation: Tu, W., X. Li, Y. Chen, G. D. Reeves, and M. Temerin (2009), Storm-dependent radiation belt electron dynamics, *J. Geophys. Res.*, *114*, A02217, doi:10.1029/2008JA013480.

1. Introduction

[2] Outer radiation belt MeV electron fluxes vary greatly during geomagnetic storms [e.g., *Baker and Kanekal*, 2008]. How such electrons are accelerated is not only interesting scientifically but also practically since MeV electrons can damage spacecraft electronics and astronauts [e.g., *Baker et al.*, 1998; *Baker*, 2001; *Fennell et al.*, 2001]. There is now some controversy as to the mechanism mainly responsible for the acceleration of outer radiation belt electrons. For some time the acceleration mechanism was mainly thought to be radial diffusion [*Fälthammar*, 1965; *Schulz and Lanzerotti*, 1974; *Brautigam and Albert*, 2000; *Li et al.*, 2001; *Barker et al.*, 2005], which conserves the first adiabatic invariant (μ) and is due to large-scale fluctuations in the magnetosphere's magnetic and electric fields acting on a preexisting positive radial gradient in the phase space densities (PSD). Recent data have shown, however, that the PSD can peak as a function of radius inside geosynchronous orbit [*Selesnick and Blake*, 2000; *Green and Kivelson*, 2004, *Iles et al.*, 2006]. Since such peaks cannot be explained by radial diffusion, a greater emphasis has recently been placed on the in situ acceleration of electrons by wave-particle interactions, which violates μ [*Horne and Thorne*, 1998; *Summers et al.*, 1998; *Meredith et al.*, 2002; *Horne et al.*, 2005a, 2005b] as a mechanism for explaining the outer electron radiation belt enhancement. The relative contribution from these two competing mechanisms has not been clear due to the lack of PSD data with appropriate temporal and spatial coverage, and the simultaneous occurrence of energization and loss. Some recent modeling works that include both radial diffusion and local acceleration have been developed. For example, *Varotsou et al.* [2005] and *Fok et al.* [2008] simulated the electron dynamics in the outer radiation belt by combining radial diffusion and wave acceleration due to whistler mode chorus waves, and they concluded that in situ acceleration by whistler mode chorus followed by inward and outward radial diffusion can populate the entire outer radiation belt at high energies. However, uncertainties still exist in the quantification of the radial diffusion coefficient and the bounce-averaged pitch angle and energy diffusion coefficients.

[3] Loss of outer radiation belt electrons is believed to be mainly due to wave-particle interactions precipitating electrons into upper atmosphere, though outward radial diffusion

[1]Laboratory for Atmospheric and Space Physics, University of Colorado, Boulder, Colorado, USA.
[2]Los Alamos National Laboratory, Los Alamos, New Mexico, USA.
[3]Berkeley, California, USA.

0148-0227/09/2008JA013480$09.00

can also produce loss [e.g., *Reeves et al.*, 1998; *Shprits et al.*, 2006]. Electromagnetic ion cyclotron (EMIC) [*Summers and Thorne*, 2003; *Meredith et al.*, 2003a; *Loto'aniu et al.*, 2006], chorus [*O'Brien et al.*, 2004; *Thorne et al.*, 2005; *Shprits et al.*, 2007] and plasmaspheric hiss [*Abel and Thorne*, 1998; *Meredith et al.*, 2006, 2007] waves can precipitate electrons. However, because of the lack of adequate observation of the waves and a clear picture of the pitch angle distribution of electrons around the loss cone, the wave precipitation processes and the associated loss rates are still not well understood.

[4] *Chen et al.* [2006] have recently published electron PSD data at fixed first and second adiabatic invariants (μ and K) using flux and field measurements from multiple satellites. Figure 1a is an example showing the PSD as a function of L^* and time ($L^* = 2\pi k/(\phi R_E)$, where ϕ is the third adiabatic invariant, k is Earth's magnetic moment and R_E is the Earth radius [*Roederer*, 1970]). This L^* is sometimes referred to as Roederer L. By tracing the temporal evolution of the PSD radial distribution for the storm starting on 16 October 2002, *Chen et al.* [2007] concluded that the radial peak in the PSD at geosynchronous orbit was caused by in situ acceleration. Furthermore, on the basis of 2 years of PSD data, they found that electron PSD peaks near $L^* = 5-6$ are common and suggested that in situ heating is likely the dominant acceleration mechanism for energetic electrons in the radiation belt. However, since the outer radiation belt dynamics are caused by a combination of the simultaneous acceleration, transport and loss processes, only by using realistic physics-based models, can we examine the distinct role of single processes and investigate their effect in combination.

[5] In this report, we compare electron PSD data from *Chen et al.* [2007] with a time-dependent radial diffusion model including finite electron lifetimes, with and without an in situ heating term, and also with a model having only in situ heating and finite electron lifetimes but without radial diffusion, to study electron acceleration mechanisms both on average and during individual storms.

2. Model Description

[6] Our model uses the Fokker-Planck equation [*Schulz and Lanzerotti*, 1974]:

$$\frac{\partial f}{\partial t} = L^2 \frac{\partial}{\partial L}\left(\frac{D_{LL}}{L^2}\frac{\partial f}{\partial L}\right) - \frac{f}{\tau} + S \tag{1}$$

where L is L^* here but we drop the asterisk here and for the rest of the equations in this paper, $f(L, t)$ is the gyro, bounce and drift phase-averaged PSD at fixed μ and K, D_{LL}, the radial diffusion coefficient, τ, the electron lifetime, and S, the heating rate. For given D_{LL}, τ and S, this equation can be solved numerically for $f(L, t)$ using, for example, the Crank-Nicolson method as is done here. In our model, we introduce simplified functional descriptions of acceleration, transport and loss with free parameters in those functions. Then we perform a least squares fit to these free parameters using the geosynchronous satellite data near $L^* = 6$ as a boundary condition to optimize the fit of the GPS PSD data near $L^* = 4$. On the basis of the comparison of the numerical magnitude of different terms and the quality of fit, we find which processes dominate during different events.

[7] For the diffusion coefficient, in order to compare with other colleagues' work, we adopt the widely used empirical form [*Shprits et al.*, 2005, 2006; *Kondrashov et al.*, 2007] $D_{LL}(Kp) = 10^{(0.506Kp\,-\,9.325)}L^{10}$ (Kp is an index, measuring magnetic activity) from *Brautigam and Albert*'s [2000] magnetic diffusion coefficient D_{LL}^M, since the magnetic diffusion coefficient is substantially larger than the electric diffusion coefficient. Their application of $D_{LL}(Kp)$ to model relatively low-energy electrons ($E < 1$ MeV) agreed well with the data. However, for higher-energy electrons ($E > 1$ MeV), their model underproduced the PSD throughout the recovery phase, indicative of an internal source or possible errors in $D_{LL}(Kp)$. Since the diffusion coefficient is, in principle, related to the global mode structure and power spectral density of the stochastic fluctuating field at electrons' drift frequency and its harmonics [e.g., *Fälthammar*, 1965; *Fei et al.*, 2006], which are difficult to determine, the form $D_{LL}(Kp)$ is only approximate. Until better information exists, the strength of radial diffusion is therefore adjusted by using a free parameter, A:

$$D_{LL} = A \times 10^{(0.506Kp-9.325)}L^{10} \tag{2}$$

where A and D_{LL} are in units of $(R_E)^2\ \mathrm{d}^{-1}$.

[8] The electron lifetime, τ, varies with magnetic activity and location and also requires careful consideration. An explicit loss term due to electron drift to the magnetopause is unnecessary in our model since the PSD at $L^* = 6$, our outer boundary, was well defined. The variation of Roederer L (L^*) with respect to the actual radial distance already incorporates or rather removes the *Dst* effect [*Li et al.*, 1997; *Kim and Chan*, 1997] from the PSD data, allowing us to focus on nonadiabatic losses due to wave-particle interactions. *Summers et al.* [2007] derived the loss timescale for the radiation belt electrons due to the combined loss effect from chorus, plasmaspheric hiss, and EMIC waves. And for calculating the pitch angle diffusion coefficient, they made some detailed assumptions on the related wave and background plasma properties. However, this report is the first attempt to empirically parameterize the electron lifetime incorporating the expected loss effects from three different waves that interact with electrons in different regions of the magnetosphere: outside the plasmasphere, inside the plasmasphere, and near the plasmapause. We calculate loss rates separately for these regions and the plasmapause is taken to be a dynamic boundary given by the empirical model of *O'Brien and Moldwin* [2003]:

$$L_{PP} = -1.57 \log_{10}\left|Dst^*\right| + 6.3 \tag{3}$$

where L_{PP} is the plasmapause location from the center of the Earth in earth radii and Dst^* is the minimum value of *Dst* during the previous 24 h. Then the three regions are defined as $L \geq L_{PP} + \Delta L_1$, outside the plasmasphere; $L_{PP} - \Delta L_1 < L < L_{PP} + \Delta L_1$, near the plasmapause and $L \leq L_{PP}$, inside the plasmasphere, where ΔL_1 provides a finite width of the effective region for the wave population acting close to the plasmapause.

[9] Outside the plasmasphere ($L \geq L_{PP} + \Delta L_1$) we consider chorus waves. *Shprits et al.* [2007] has parameterized the

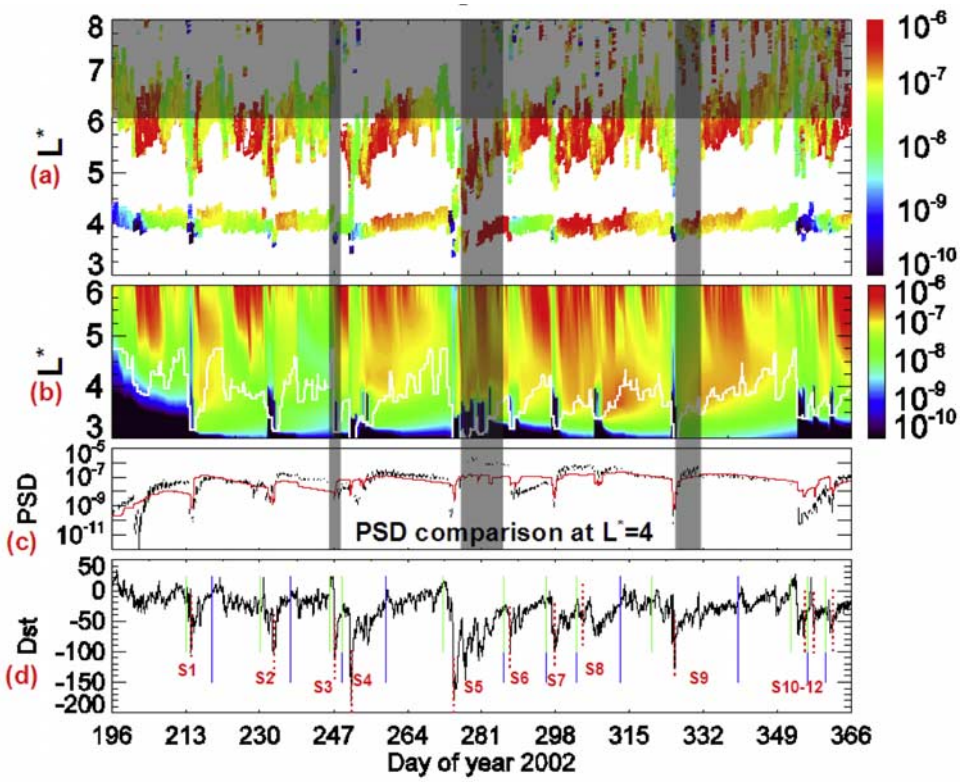

Figure 1. (a) Phase space densities (PSD) data for $\mu = 2083$ MeV G^{-1} and $K = 0.03G^{1/2}R_E$ from day of year (DOY) 196 to 365 of 2002. PSD is in units of $(c\ \text{MeV}^{-1}\ \text{cm}^{-1})^3$. The data between $L^* = 6$ and 8 are shaded for better comparison with Figures 1b and 1c. Gray areas correspond to data gaps in the PSD at $L^* = 6$ (outer boundary of the model). (b) Model results with radial diffusion, internal heating and losses. The white curve shows the plasmapause location. (c) PSD comparison between data (black curve) and model results (from Figure 1b, red curve) at $L^* = 4 \pm 0.2$. (d) *Dst* data with all 12 storms marked (green vertical line, the storm start; blue vertical line, the storm end; red dotted line, the turned-on time for internal heating, which is given by equation (10).)

loss timescale of radiation belt electrons due to chorus waves as a function of the geomagnetic index, *AE*:

$$\tau_{\text{Chorus}} = 4.8 \times 10^4 B_w^{-2} L^{-1} E^2, \tag{4}$$

with

$$B_w^2 = 2 \times 10^{1.7+2.3\times10^{-3}AE^*} pT^2, \tag{5}$$

where τ_{Chorus} is the electron lifetime in days, B_w, the total wave amplitude in pT, E, the kinetic energy of the electrons in MeV, and AE^*, the maximum value of the *AE* index during the previous 3 h. For electrons mirroring near the equator and for a given μ in MeV G^{-1}, energy, E, can be expressed as a function of dipole L, which is approximated as L^* in our model, and then the loss timescale is approximated as

$$\tau_{\text{Chorus}} = C \times 2.4 \times 10^{2.3-2.3\times10^{-3}AE^*} \cdot L^{-1}\left(\sqrt{0.512^2 + 0.307\mu L^{-3}} - 0.512\right)^2 \text{ days} \tag{6}$$

C is introduced as a free parameter to adjust the lifetime outside the plasmasphere and compensate for the uncertainties in equation (4). For $C = 1$, $AE^* = 900$ nT, $\mu = 2083$ MeV G^{-1} (as in our case), $\tau_{\text{Chorus}} \approx 1.1$ days at $L^* = 6$ and ≈ 7.4 days at $L^* = 4$.

[10] Losses inside the plasmasphere are mainly caused by resonance with plasmaspheric hiss on timescales on the order of 10 days, and scale with geomagnetic activity [*Abel and Thorne*, 1998; *Meredith et al.*, 2004]. Since there is no well-parameterized form of electron loss timescale due to plasmaspheric hiss and since the electron lifetime inside the plasmasphere is not critical for our current model because the PSD data we use are for electrons at $L^* \geq 4$, which stay mostly outside the plasmasphere, we set the electron lifetime, for simplicity, inside the plasmasphere uniformly as:

$$\tau_{\text{hiss}} = 10 \text{ days}. \tag{7}$$

[11] EMIC waves may cause rapid dropouts of relativistic electrons on timescale of hours during storms [*Meredith et al.*, 2003a; *Albert*, 2003] and may be preferentially generated near the plasmapause where the ring current overlaps the cold dense plasmasphere [*Fraser and Nguyen*, 2001]. Therefore we assume that the EMIC-active region is close to the plasmapause. Recently, *Engebretson et al.* [2008] noted that there is yet little ground-based evidence for the occurrence of EMIC waves during the storm main phase. Although this could perhaps be explained by the failure of

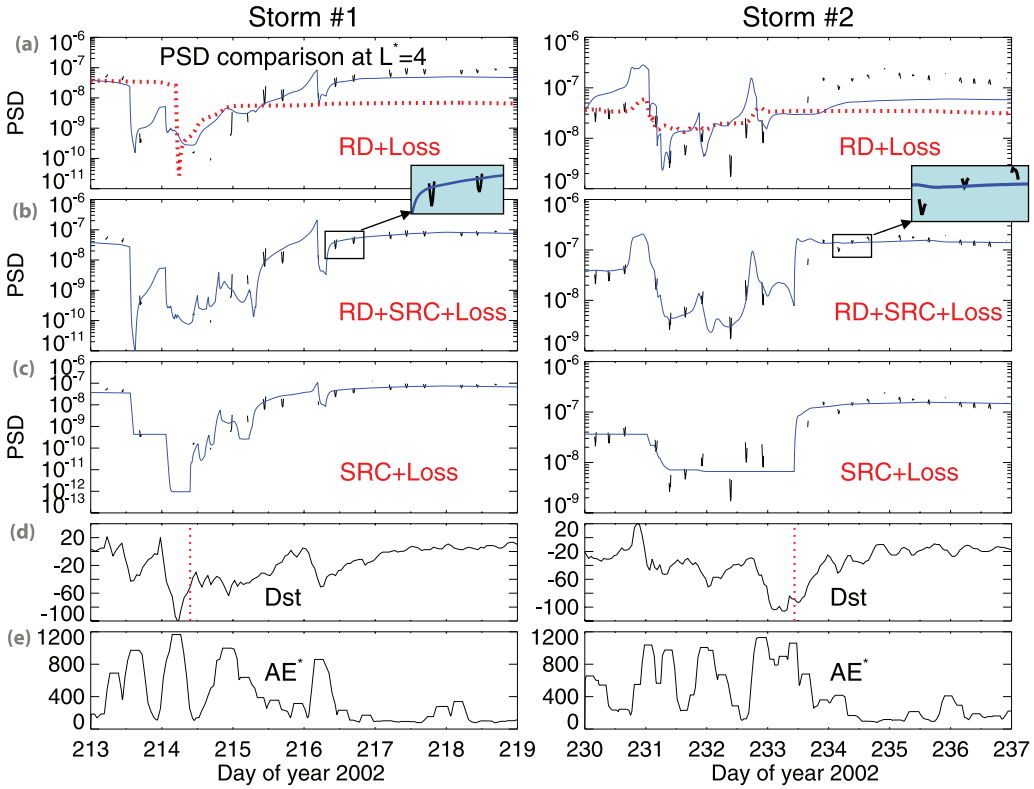

Figure 2. Comparison between PSD data and model results at $L^* = 4 \pm 0.2$ for two storms, 1 and 2. (left) Storm 1 from DOY 213/2002 to DOY 219/2002. In Figures 2a (left)–2c (left), black curves are PSD data, solid blue lines are model results. In Figure 2a (left) (RD only + Loss), dotted red line is RD($A = 1$) + Loss; solid blue line is $RD_{enh}(A > 1)$ + Loss. Figure 2b (left) is model results with RD_{enh} + Source + Loss; Figure 2c (left) is Source only + Loss. The *Dst* and *AE** time profiles are plotted in Figures 2d and 2e. (right) Storm 2 from DOY 230/2002 to DOY 237/2002 with the same configuration. The V and inverted V shapes (explicit in squared zoom-in regions in Figure 2b (left) and Figure 2b (right)) indicate the radial gradient of the PSD (V shape, positive gradient; inverted V, negative gradient).

EMIC waves to propagate from space to the ground, it remains controversial whether EMIC waves are the dominant loss process for the outer radiation belt electrons during magnetic storms. However, fast electron precipitation during the storm main phase is observed [*Iles et al.*, 2002; *Selesnick*, 2006], indicating that some intense wave activity must be present to account for the strong pitch angle diffusion of electrons. This is consistent with the often observed sudden dropouts of PSD data at $L^* = 4$ at specific times when *Dst* falls below a certain value (see the black curve in Figure 1c and the black sporadic data curve in Figure 2a (left)). Since our paper is not aiming to identify the role of possible loss mechanisms, we simply simulate the observed fast loss to the first-order approximation with a free parameter. We also introduce the critical *Dst* parameter, Dst_{cri}, which effectively determines when significant losses take effect. This is an important assumption in our model. Then, when $Dst < Dst_{cri}$, we parameterize the electron lifetime close to the plasmapause separately, scaling with the storm index, *Dst*:

$$\tau_{fastLoss} = \tau_0 / \left(\frac{Dst}{-50\ \text{nT}} \right) \tag{8}$$

where τ_0 is a free parameter to adjust for this fast loss during the storm main phase and to compensate for the uncertainty introduced by this simplified loss term.

[12] Thus, the final form for the electron lifetime in our model is

$$\begin{cases} L \geq L_{PP}: \tau = C \times 2.4 \times 10^{2.3 - 2.3 \times 10^{-3} AE^*} L^{-1} \left(\sqrt{0.512^2 + 0.307 \mu L^{-3}} - 0.512 \right)^2 \text{days} \\ L < L_{PP}: \tau = 10 \text{ days when } Dst < Dst_{cri},\ \tau = \tau_0 / (Dst/ - 50\ \text{nT}) \text{ at } L_{PP} - \Delta L_1 < L < L_{PP} + \Delta L_1 \end{cases} \tag{9}$$

[13] Now we specify the heating term. *Meredith et al.* [2002] suggested that electron acceleration occurs in the presence of enhanced chorus waves, mostly during storm recovery phases containing prolonged substorm activity.

Since acceleration is most efficient just outside the plasmapause [*Horne et al.*, 2005b], we add a heating term during the storm recovery phase (from 4 h after the minimum of *Dst* until the end of a storm) just outside the plasmapause. (A storm is identified when *Dst* falls below −50 nT. After acquiring the local minimum *Dst* point, the storm interval for our modeling purposes is defined as: starting point: 1 day before the first zero *Dst* point before the local minimum *Dst*; end point: the recovery of *Dst* to zero. *Dst* dips more than 3 days apart during one storm interval are counted as separate storms, with the end of one storm defined as the next *Dst* peak, which is also the start of the next storm.) According to the model results of *Shprits et al.* [2007], chorus wave amplitudes can be parameterized as a function of AE^* as in equation (5), which can be used to specify our internal source term. But the parameterization for the chorus amplitudes in equation (5) is based on the wave observation of dayside chorus (0600–1500 magnetic local time (MLT)) at latitudes between 20° and 30° that was specifically constructed to estimate loss rates [*Shprits et al.*, 2007], and local heating is expected to be more efficiently excited by equatorial nightside chorus [*Li et al.*, 2007]. However, *Meredith et al.* [2003b] suggested that the intensity of off-equator chorus waves in the predawn sector is qualitatively comparable to that of near-equator chorus in the morning sector based on spacecraft measurements. And *Meredith et al.* [2003c] also showed that relativistic electron flux enhancements were correlated with increased magnetic activity as monitored by the *AE* index. Therefore, because of the uncertainties in the wave parameterization caused by inadequate wave observations with decent spatial and temporal coverage and resolutions, current unavailability of the parameterization for nightside chorus intensity, and the fact that our model simulated the gyro, bounce and drift phase-averaged PSD (the wave heating by chorus both on the dayside and nightside needs to be drift phase (or MLT) averaged), we still define our source term as proportional to the wave amplitude in equation (5) and as a function of *AE* index:

$$S = \begin{cases} S_0 \times B_w^2 = S_0 \times 2 \times 10^{1.7+2.3\times10^{-3}AE^*} & (L_{PP} < L < L_{PP} + \Delta L_2) \\ 0 & (\text{other } L \text{ regions}) \end{cases} \quad (10)$$

where S_0 is the scaling factor of the magnitude of the internal source, which is also used to compensate for the uncertainties in the source term, and ΔL_2 defines a finite region of local heating.

[14] To summarize, the free parameters in our model are: *A*, the scaling factor for the diffusion rate; Dst_{cri}, the *Dst* based critical parameter; *C*, the chorus scaling factor; τ_0, the EMIC scaling factor; ΔL_1, the effective width for EMIC wave measured in Earth radii; S_0, the internal source rate scaling factor in (c MeV^{-1} cm^{-1})^3 d^{-1} since PSD is in (c MeV^{-1} cm^{-1})^3 and ΔL_2, the width of internal heating in Earth radii.

[15] Using this model we simulated the PSD variation between $L^* = 2.5$ and $L^* = 6$. We compared the logarithm of the model results and the PSD data around $L^* = 4$. The model performance was measured by the prediction efficiency (PE) [*Li et al.*, 2001] and the linear correlation coefficient (LC) (alternatively, the covariance of the two vectors) over the defined interval. Specifically, PE is defined as

$$\mathrm{PE} = 1 - \frac{\text{mean square residual}}{\text{variance of data}} = 1 - \frac{\sum_i^n (d_i - p_i)^2}{\sum_i^n \left(d_i - \bar{d}\right)^2},$$

where d_i and p_i are the data and model results, respectively, and $\bar{d}$ is the mean of all d_i (PE = 0: model results are as good as the averaged data, $p_i = \bar{d}$; PE > 0: the model is better than reproducing the average and PE = 1: perfect modeling). Since we actually compared with the PSD data over $L^* = 4 \pm 0.2$ (and assumed they are at $L^* = 4$) to include enough statistics without being too wide, our model results were also averaged over $L^* = 4 \pm 0.2$.

[16] One thing we would like to clarify is that our model approach is different from the wave study approach of using energy and pitch angle diffusion to study the outer radiation belt dynamics [e.g., *Shprits et al.*, 2007; *Li et al.*, 2007]. They are complementary approaches, both of which have to assume parameters. For example, the *Li et al.* [2007] work assumes the spectral distribution of the wave power, the ratio of plasma frequency to electron gyrofrequency (f_{pe}/f_{ce}), the distribution of wave normal angles, local time content etc, but then uses the full Fokker-Planck solution. But our model, based on parameter fitting, approximates the effects of energy and pitch angle diffusion without explicitly using these diffusion coefficients. An advantage, however, is that it can estimate the effects of many simultaneous processes as shown in section 3.

3. Model Results

[17] The model was run between $L^* = 2.5$ and $L^* = 6$, with $\mu = 2083$ MeV G^{-1} (corresponding to $E \sim 1.3$ MeV at $L^* = 6$ and 2.7 MeV at $L^* = 4$) and $K = 0.03G^{1/2}\ R_E$ (equatorial pitch angle near 90°) from 15 July 2002 to 31 December 2002. The PSD at the inner boundary was fixed at $f(L = 2.5) = 10^{-15}$ (c MeV^{-1} cm^{-1})^3 to denote the low flux in the slot region. The outer boundary was set to the PSD data averaged over $5.5 < L^* < 6.5$ with a time resolution of 10 min (Here the PSD gradient over L^* is less steep than near $L^* = 4$ based on the data in Figure 1a and so we can average over a wider L^*.) We interpolated across data gaps. For the initial condition we interpolated across L^* using the available PSD data at $L^* = 6$ (from LANL satellites) and $L^* = 4$ (from GPS satellites).

[18] We first ran the model for the whole second half of 2002. There were 12 storms during this period based on the storm definition in the previous section, which are marked in Figure 1d (*Dst* profile, green vertical line denotes the start of a storm; blue vertical line denotes the end). The heating turn-on time for each storm (4 h after the minimum *Dst*) is indicated by the vertical red dotted line. The heating lasts until the end of the storm. After adjusting all the parameters,

Table 1. Optimum Parameter Values and Corresponding PE and LC for the Half-Year Run

	A	Dst_{cri} (nT)	C	τ_0 (days)	ΔL_1	τ_{hiss} (days)	$S_0 \times 10^{10}$	ΔL_2	PE	LC
Values	0.668	−66.8	0.1089	0.0011	0.6087	10[a]	0.242	2.7504	0.477	0.693

[a]Fixed parameter.

the maximum PE for the long-term run was 0.477. The corresponding parameter values are shown in Table 1. The model results are illustrated in Figure 1b and the comparison between the model results and the PSD data at $L^* = 4$ is depicted in Figure 1c. Vertical gray areas in Figure 1 are gaps in the PSD data at $L^* = 6$ (the outer boundary of our model) where we interpolated to get the boundary values, during which (and sometime beyond) the model results are not valid. Worth mentioning is that ΔL_2, the width of the local heating region, was 2.75 (see Table 1), indicating that local heating was needed almost across the entire region from the plasmapause (illustrated by the white curve in Figure 1b) to the outer boundary ($L^* = 6$). Overall, the model fairly well captured the general PSD variations, but with overprediction and underprediction at different times.

[19] From Figure 1c it is clear that the model does not simulate correctly some of the PSD dropouts at $L^* = 4$ (e.g., the PSD dropout in storm 5, around day of year (DOY) 274). One possibility is that the *Dst* effect was not totally removed from the PSD data for such times. Although, the variation of L^* for the PSD data should have incorporated the *Dst* effect, possible errors from imperfect magnetic field models or poor assumptions of particle pitch angle distributions could still have created some *Dst* effect, especially near $L^* = 4$ where the PSD has a steep gradient. Another possibility lies in an error in L_{PP} (equation (3)), the plasmapause location from the center of the Earth. This dynamic boundary defines the three loss regions. However, our model uses the Roederer L coordinate and we take L_{PP} to be Roederer L. This approximation may lead to incorrect losses in our model and may degrade the model performance. The most important influence of L_{PP} is on the EMIC-loss region ($L_{PP} - \Delta L_1 < L < L_{PP} + \Delta L_1$), which creates the fast loss of electrons. Because of the possible errors of L_{PP}, the turn-on of fast EMIC loss near the plasmapause with the same value of ΔL_1 can locally lead to a poorer performance of our model. In individual storm studies we can compensate for the offset of the estimated L_{PP} since for each storm we can use a different ΔL_1 value.

[20] The model sometimes also underpredicted the PSD at $L^* = 4$. For example, during the recovery phases of storm 7 (around DOY 298), the modeled PSD was less than the PSD data with the internal heating turned on, which means the modeled internal source was not strong enough. The simulation can be improved by increasing S_0, the internal source scaling factor, during such storms. On the other hand, for example during the interval between storm 4 and storm 5, when there is no internal heating, the model underpredicted the PSD at $L^* = 4$ possibly because the model radial diffusion was not strong enough during that time. By increasing A, the diffusion rate scaling factor, the results can be improved. Thus, the same set of parameters could not be applied to all storms and the relative contribution of radial diffusion and internal heating seemed to vary from storm to storm.

[21] On the basis of the above analysis of the long-term run, we realized that a simulation of individual storms would be interesting. Therefore, we simulated individually four storms in the second half of 2002: storms 1, 2, 4, and 7. We choose these storms because they lasted long enough ($\geq$6 days) to include sufficient data; there were no large data gaps at the outer boundary; and the PSD was enhanced after the storm. First, in order to investigate the relative contribution from radial diffusion, internal heating and loss, we modeled each storm without the heating term ($S_0 = 0$). Such a model shows the behavior of the electron population at $L^* < 6$ from just radial diffusion and loss. Two such runs were done. For the first run, A, the diffusion scaling factor, was set to one in equation (2) and the other parameters were adjusted. For the second run, A was made adjustable. The results of these two runs indicate how well these storms can be simulated by only radial diffusion and losses. Then the heating term was included to investigate the significance of internal heating. Finally, we reduced radial diffusion to zero ($A = 0$) and simulated the storms with only an internal source plus loss.

[22] For each run all adjustable parameters were determined by maximizing the PE. The optimum values are shown in Tables 2 to 5. The corresponding PEs and LCs are also shown together with S_{ave} (unit (c MeV^{-1} cm)^3 d^{-1})), the average heating rate outside the plasmapause over the heating period (between the red dotted line and blue solid line of corresponding storm in Figure 1d) since the internal source S varies as a function of AE^*. Comparing the parameters across all the runs, we found that the chorus loss scaling parameter, C, was sometimes 1000 or essentially infinite lifetime or no loss from chorus. Now we discuss the model results for storms 1 and 2 in detail.

Table 2. Optimum Parameter Values and Corresponding PE and LC for Each Run of Storm 1[a]

	Run	A	Dst_{cri} (nT)	C	τ_0 (days)	ΔL_1	τ_{hiss} (days)	S_0 ($\times 10^{10}$)	S_{ave_7} ($\times 10^7$)	ΔL_2	PE	LC
R1	RD + Loss	*1.0*	−95.4	1000	0.0113	1.0698	*10*	*0*	-	-	**0.025**	**0.364**
R2	RD_{enh} + Loss	8.933	−46.4	0.0498	0.0049	0.5922	*10*	*0*	-	-	**0.856**	**0.960**
R3	RD_{enh} + SRC + Loss	10.583	−46.4	0.1456	0.0048	0.9549	*10*	1.789	**3.418**	0.4612	**0.948**	**0.974**
R4	SRC + Loss	*0*	−48.9	1000	0.0115	0.6679	*10*	1.078	**2.060**	0.6717	**0.910**	**0.958**

[a]Numbers in italic type are nonadjustable parameters; numbers in bold type indicate calculated values; and the rest are free parameter values. RD, radial diffusion with $A = 1$; RD_{enh}, enhanced radial diffusion with $A > 1$; SRC, internal source.

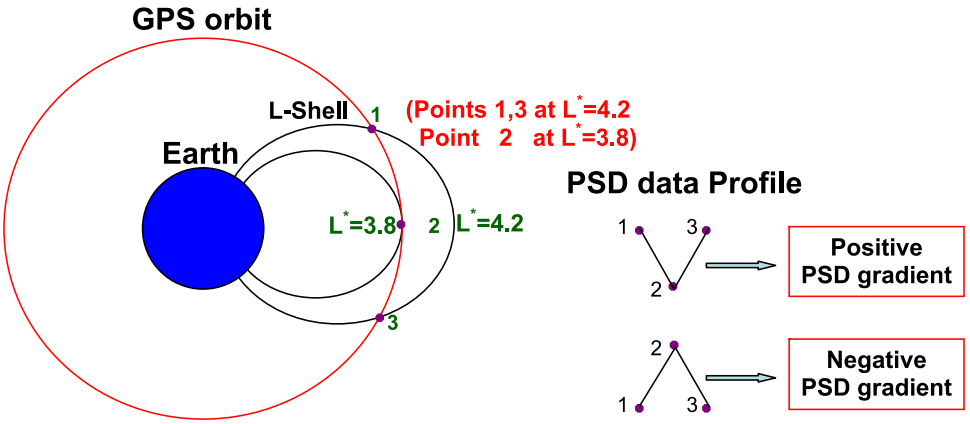

Figure 3. The correspondence between the shape of the PSD data at $L^* \approx 4$ and the local PSD gradient. V shape, positive gradient; inverted V shape, negative gradient.

[23] First, we ran our model for storm 1 without internal heating ($S_0 = 0$). The best modeled PSD at $L^* = 4$ for $A = 1$ (the red dotted line in Figure 2a (left)) has a PE of only 0.025. A comparison with the PSD data at $L^* = 4$ (the sporadic black curve) shows that radial diffusion with $A = 1$ is not strong enough to explain the enhanced PSD, especially during the storm recovery phase. Increasing radial diffusion (i.e., increasing A) gave the results shown as the blue solid line in Figure 2a (left), better reproducing the PSD data (PE = 0.856). The losses for this run were larger than the "$A = 1$" run as indicated by the smaller C and τ_0 values for R2 in Table 2. Increasing A greatly improved the simulation, indicating that a sufficient source existed at the outer boundary and that the dynamics of electrons in the inner magnetosphere ($L^* = 4$) could be explained from variations at the outer boundary ($L^* = 6$) propagating inward through radial diffusion. Thus radial diffusion could be the main acceleration mechanism for this storm. This is also consistent with the radial gradient of the PSD at $L^* \approx 4$, indicated by the V shape of the PSD data (zoomed in region in Figure 2b (left)) inferred from the passage of GPS satellites near their minimum L^*. Since the PSD data are actually covering $L^* = 4 \pm 0.2$, considering the schematic geometry shown in Figure 3, the V shape implies that the PSD increases with L^*, in agreement with the positive PSD gradient required for inward radial diffusion to be effective in increasing the PSD.

[24] Although this case could be well simulated by only enhanced radial diffusion and losses, we cannot exclude the possibility of significant local heating inside $L^* = 6$ partly compensated by larger losses, since the positive PSD gradient at $L^* = 4$ could also be explained by a local peak in the PSD at larger L^* but inside $L^* = 6$, given that peaks in the PSD in the region $5 < L^* < 6$ are common [*Chen et al.*, 2007]. Therefore, we included an internal source (the turn-on time of the source is indicated by the red vertical line in the *Dst* profile of storm 1, 4 h after minimum *Dst*) and readjusted the radial diffusion and losses to obtain the best PE. The results are shown as the blue line in Figure 2b (left) with a PE = 0.948. A comparison of "RD_{enh} + Loss" and "RD_{enh} + Source + Loss" runs of this storm based on R2 and R3 values in Table 2 shows that the other loss parameters are almost comparable except that the fast EMIC loss region is wider in the RD_{enh} + Source + Loss run. Larger losses then require increased radial diffusion ($A \approx 8.9$ for R2 to $A \approx 10.6$ for R3) to best simulate the PSD variations even though internal heating is included. Internal heating seemed to help only a little in reproducing the PSD enhancement for this case given the enhanced radial diffusion.

[25] It is also interesting to investigate how well the PSD can be simulated using only internal heating and losses. Figure 2c (left) (PE = 0.910) shows the best result with $A = 0$ (no radial diffusion). Though one might have expected this run, "Source + Loss," to have a larger internal source than RD_{enh} + Source + Loss, according to the R4 values in Table 2, it had both smaller internal sources and losses (C and τ_0 are bigger than for R3). One explanation is that strong radial diffusion removes electrons from a heating region close to $L^* = 4$, thus requiring a stronger source. Also worth mentioning is the parameter C. For the first run PE was larger when C was larger (that is why we set $C = 1000$ or effectively infinite), and even better with C negative. This indicates that there was probably some in situ heating farther outside the plasmapause for this case. In the last run (R4 in Table 2), PE was very insensitive to C, staying at 0.910 for C between 10 and 10,000. Since this storm can be well reproduced either by RD_{enh} + Loss, RD_{enh} + Source + Loss, or Source + Loss, we cannot conclude which mechanism is dominant. Although either enhanced radial diffusion (with $A > 1$) or internal heating can account for the PSD at $L^* = 4$, the results are better when both mechanisms work together.

[26] The second example is storm 2. Again, in Figure 2a (right) the dotted red line is the model results at $L^* = 4$ without any in situ source and $A = 1$. The sporadic black line shows the PSD data. Even with a significantly larger radial diffusion ($A = 23.218$) (the blue line in Figure 2a (right)) the model still underpredicted the PSD data during the storm recovery phase (PE = 0.430, Table 3), indicating that there was not a sufficient source at the outer boundary and thus an internal source is required. With the source turned on at the time of the red vertical line in the *Dst* profile, and with a different set of parameters (R3 in Table 3), the results fit the PSD data at $L^* = 4$ well as shown by the blue line in Figure 2b (right). For this run PE increased as ΔL_2, the width of internal heating, became wider and only stopped

Table 3. Same as Table 2 but for Storm 2

	Run	A	Dst_{cri} (nT)	C	τ_0 (days)	ΔL_1	τ_{hiss} (days)	S_0 ($\times 10^{10}$)	S_{ave} ($\times 10^7$)	ΔL_2	PE	LC
R1	RD + Loss	*1.0*	−33.9	1000	0.0503	0.4597	*10*	*0*	-	-	**0.172**	**0.757**
R2	RD_{enh} + Loss	23.218	−45.3	1000	0.0063	0.5664	*10*	*0*	-	-	**0.430**	**0.688**
R3	RD_{enh} + SRC + Loss	11.910	−42.9	0.0437	0.0417	0.6631	*10*	1.563	**1.420**	2.35	**0.945**	**0.972**
R4	SRC + Loss	*0*	−41.1	1000	0.0886	0.4579	*10*	0.549	**0.499**	1.05	**0.906**	**0.952**

increasing when ΔL_2 reached 2.35 (probably the outer boundary), indicating that a wide internal source is needed for this storm. During this storm's recovery phase the PSD profile had "inverted V" shapes, implying a PSD peak inside $L^* = 4$. One can even see a change of the wedge shapes from V to inverted V shapes (zoomed-in region in Figure 2b (right)) indicating a temporal evolution of the direction of PSD radial gradient from positive to negative during the storm (see Figure 3 for illustration).

[27] Results of internal heating only plus losses are shown in Figure 2c (right) (PE = 0.906). Again without radial diffusion a smaller rather than a larger internal source with smaller losses gave the optimum results. Again, a wide internal source was needed for this run. PE increased as ΔL_2 increased until ΔL_2 reached 1.05. There is a simple explanation for this based on the consideration that without radial diffusion different L shells act independently. Similar to "RD + Loss" case of storm 1, PE was larger for larger C and was even better for negative C, meaning that some internal heating extended well outside the plasmapause. For the RD_{enh} + Source + Loss and Source + Loss cases, PE was insensitive to the value of C.

[28] The parameter values and results for storms 4 and 7 are shown in Tables 4 and 5 and Figure 4. Both these two storms can be well reproduced by enhanced radial diffusion only plus some losses (the blue curves in Figures 4a (left) and 4a (right) with PE = 0.780 and 0.876 respectively), which agree with the successive V shapes shown in the PSD profile during the time when PSD is increasing (zoomed-in boxes in Figures 4b (left) and 4b (right)). With internal sources, both cases were better simulated. For storm 4 radial diffusion decreased (A from 3.275 to 0.143 in Table 4) but for storm 7 it increased because of faster losses (comparing R2 and R3 in Table 5) in order to obtain the highest PE. Since storm 4 is a big storm with a sharp narrow Dst dip (minimum Dst reached ∼−190 nT), its optimum Dst_{cri} value was smaller than that for the other storm; the L_{PP} value was smaller; and the width of fast EMIC loss region was bigger (see Table 4). Also the Source + Loss runs could reproduce the PSD variations in these two storms. Again, both cases were best simulated with both radial diffusion and internal heating acting together (RD_{enh} + Source + Loss). However, a comparison of A, the diffusion rate scaling factor, and S_{ave}, the average heating rate (R3 in Tables 4 and 5) shows that the relative contribution from the

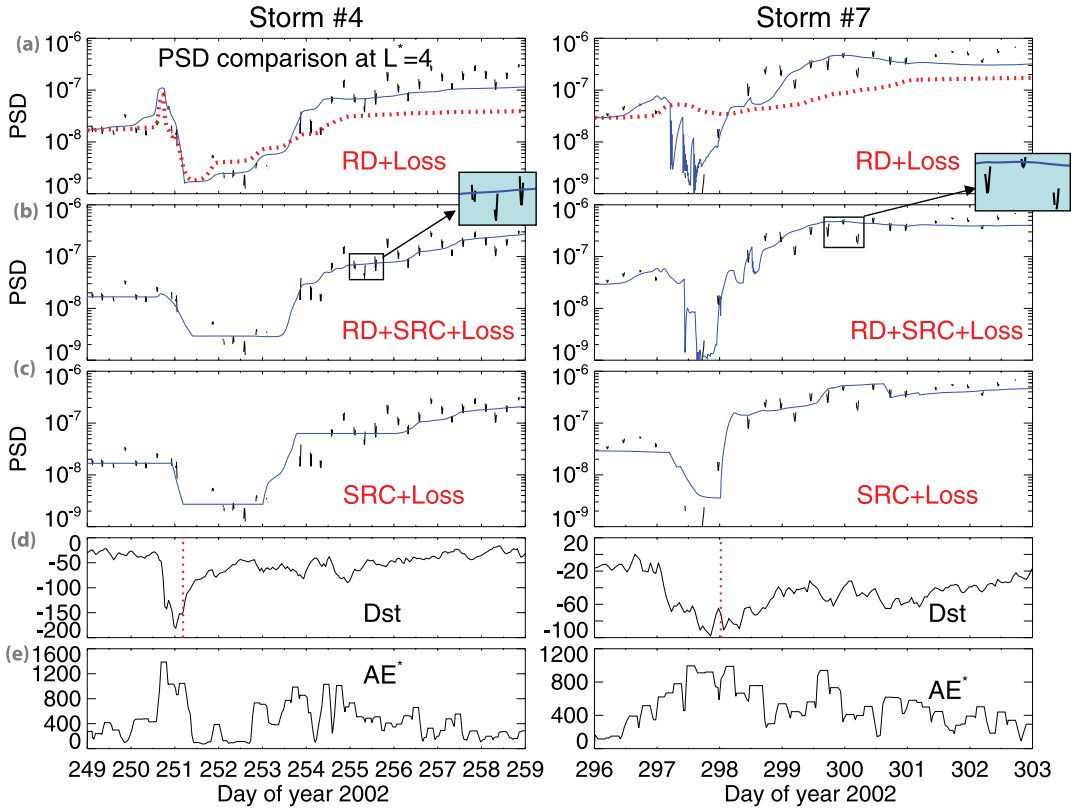

Figure 4. Comparison between PSD data and model results at $L^* = 4 \pm 0.2$ for other two storms, 4 and 7. The configuration is the same with Figure 2.

Table 4. Same as Table 2 but for Storm 4

	Run	A	Dst_{cri} (nT)	C	τ_0 (days)	ΔL_1	τ_{hiss} (days)	S_0 ($\times 10^{10}$)	S_{ave} ($\times 10^7$)	ΔL_2	PE	LC
R1	RD + Loss	*1.0*	−90.2	1000	0.0648	1.3358	*10*	*0*	-	-	**0.500**	**0.867**
R2	RD_{enh} + Loss	3.275	−127.4	1000	0.1527	2.7200	*10*	*0*	-	-	**0.780**	**0.885**
R3	RD_{enh} + SRC + Loss	0.143	−93.7	0.3925	0.7131	2.6002	*10*	1.702	**4.713**	0.3609	**0.904**	**0.951**
R4	SRC + Loss	*0*	−148.1	1000	0.4580	1.4100	*10*	1.056	**2.924**	0.4232	**0.851**	**0.923**

two acceleration mechanisms was very different. Although the loss parameters differed, with a comparable average internal source storm 7 required much stronger radial diffusion than storm 4.

[29] In summary, of the four storms, three could be well reproduced either by acceleration from radial diffusion or from internal heating only, though the best results were achieved using both. The other storm clearly required additional local heating to account for the enhancement of the PSD. Different storms required different relative magnitudes of radial diffusion and internal heating. Therefore, one conclusion is that the relative contributions of radial diffusion and internal heating responsible for the enhancement of radiation belt electrons vary from storm to storm.

4. Discussion

[30] In individual storm studies we have simulated each storm using four different runs. In one storm (storm 2) the source term is definitely dominant but in the other three storms both RD_{enh} + Loss and Source + Loss give fairly reasonable results, although the PE for Source + Loss is bigger than the PE from RD_{enh} + Loss for all four storms. That means that both RD_{enh} + Loss and Source + Loss can account for the increase in the electrons. Thus, the study of outer radiation belt dynamics only based on PSD data interpretation is accompanied with some uncertainties, which further proves the benefit of modeling efforts. And as we discussed, the most physical case is when both radial diffusion and internal heating are acting together, or the RD_{enh} + Source + Loss run. But how to decide which acceleration mechanism contributes more? For this we need to compare this run with the other two runs, Source + Loss and RD_{enh} + Loss. The results (Tables 2–5) show that from the run Source + Loss to the run RD_{enh} + Source + Loss, the source term increases; while from the run RD_{enh} + Loss to the run RD_{enh} + Source + Loss, the radial diffusion term generally decreases or stays the same (except for storm 1 and that is only a small increase in A). If we consider the value of source in the Source + Loss run as the necessary amount of source to reproduce the electron enhancement and the radial diffusion strength in the RD_{enh} + Loss run as the necessary strength of radial diffusion, the results mean that in the RD_{enh} + Source + Loss run there is even more source than necessary to account for the increase in the electrons while there is often less radial diffusion than necessary to account for the electron enhancement. On the basis of these, we conclude that internal source term contributes more.

[31] Comparing results from all four storms, we found that radial diffusion with $A = 1$ is never enough to reproduce the PSD enhancement during the storm recovery phase. The A values in RD_{enh} + Loss runs are 8.9, 23.2, 3.3, and 7.6 for four storms and in the RD_{enh} + Source + Loss runs $\approx$ 10.6, 11.9, 0.143, and 7.6, that is, averaging around 10, substantially larger than one would have expected from the results of *Brautigam and Albert* [2000]. This is interesting, since if $D_{LL}(Kp)$ with $A = 1$ worked well in Brautigam and Albert's model for lower-energy electrons, for higher-energy electrons the diffusion coefficient should be even smaller ($A <$ 1) since electrons with higher energies have higher drift frequencies and resonate with ULF waves at higher frequencies which have less power. So how to reconcile the large values of the radial diffusion coefficients? Radial diffusion makes a connection between the boundary conditions at $L^* = 6$ and the PSD at $L^* = 4$. But there is more than one way to make this connection other than radial diffusion at constant first and second adiabatic invariants. We know that low- and high-energy electrons at $L^* = 6$ are well correlated (with high-energy electrons delayed with respect to low energy [*Li et al.*, 2005; *Turner and Li*, 2008]), and the lower-energy electrons at $L^* = 6$ can be transported to $L^* = 4$ faster, either by direct convection or by faster diffusion. Such lower-energy electrons at $L^* = 4$ can act as source for local heating. Putting these points together gives us a model for the connection of higher-energy electrons between $L^* = 6$ and $L^* = 4$ that mimics radial diffusion but is much faster. (Of course assuming that the real radial diffusion is smaller makes the source term even more dominant.) This gives a possible explanation for the large values of radial diffusion coefficient.

[32] Now we discuss the parameter sensitivity of our model. We varied each of the loss term tunable parameters (Dst_{cri}, C, τ_0, ΔL_1 and τ_{quiet}) by ±20% for RD_{enh} + Loss run of storm 1. The PEs changed within ±0.01 with respect to changes of all the loss-related parameters except for ΔL_1 (PE decreased to 0.67 when ΔL_1 changed to 0.8) and Dst_{cri} (PE = 0.68 when $Dst_{cri} = -38.0$). ΔL_1 is a sensitive parameter since it defines the finite region of EMIC wave loss whose time scale is much shorter than of the other losses (see Table 2). The model is also sensitive to Dst_{cri} because it is critical to turning on the fast storm time losses. For the same run, we also checked the sensitivity of our model to the electron lifetime due to plasmaspheric hiss,

Table 5. Same as Table 2 but for Storm 7

	Run	A	Dst_{cri} (nT)	C	τ_0 (days)	ΔL_1	τ_{hiss} (days)	S_0 ($\times 10^{10}$)	S_{ave} ($\times 10^7$)	ΔL_2	PE	LC
R1	RD + Loss	*1.0*	no loss	no loss	no loss	no loss	no loss	*0*	-	-	**0.242**	**0.712**
R2	RD_{enh} + Loss	7.594	−66.0	1000	0.0008	0.6604	*10*	*0*	-	-	**0.876**	**0.941**
R3	RD_{enh} + SRC + Loss	7.614	−69.9	0.0258	0.0013	0.8104	*10*	2.265	**5.936**	2.0154	**0.930**	**0.966**
R4	SRC + Loss	*0*	−61.7	1000	0.2364	0.7533	*10*	0.863	**2.262**	0.8459	**0.881**	**0.939**

τ_{hiss}, which was assumed to be 10 days. PE was very insensitive to τ_1, which varied within ±0.03 when τ_1 changed from 1 day to 100 days, ensuring the validity of our assumption. This is because the plasmapause is mostly inside $L^* = 4$, where the PE is calculated, during storms. To consider the effect of the delay time (4 h) to turn on the internal source after the *Dst* minimum, we selected the RD_{enh} + Source + Loss run for storm 1. The PE varied within ±0.001 as the delay time varied from 0 to 6 h with the highest PE for 4 h.

[33] Next we discuss the possible sources of error involved in our modeling efforts. The first is from our database: the PSD data from *Chen et al.* [2007]. Possible error sources in the PSD calculation, such as the imperfect magnetic field model and poor assumption of particle pitch angle distribution, can lead to some uncertainties in our conclusions. *Chen et al.* [2007] chose the T01s model for PSD calculations because its statistical performance was best during the storm times and made effort to construct instrument intercalibration to constrain all these errors.

[34] Another possible error source is in the auxiliary models, such as the empirical form of diffusion coefficient from *Brautigam and Albert* [2000], the parameterized electron lifetime due to chorus wave from *Shprits et al.* [2007] and the estimated plasmapause location from *O'Brien and Moldwin* [2003]. Inaccuracy in these models will limit our model performance. To investigate the sensitivity of our model to the performance of these auxiliary models is an important part of our future work.

[35] Our model uses some simplified assumptions. First, electron losses are divided into three regions, because there are likely three different wave populations that interact with electrons depending on the region. It is assumed that chorus waves are most effective outside the plasmasphere, EMIC waves dominant close to the plasmapause and plasmaspheric hiss inside the plasmasphere. Since the properties of EMIC waves are not yet well known, we set a free parameter in our model (equation (8)) for the loss rate from EMIC waves or whatever waves leading to loss of electrons near the plasmapause. The form of plasmaspheric hiss loss is somewhat oversimplified in the current model. However, it does not play a significant role in our model performance so far because of its relatively slow loss rate. Simple as the assumption is, our loss term reasonably represents the main wave loss processes in the radiation belt and has worked well. The second simplified assumption is the time and region limited internal source. Admittedly, local heating can also happen sporadically during the storm main phase and over extended L^* regions. However, our simplified form of the internal source is capable of representing the main characteristics of in situ heating. Additionally, our internal source term is parameterized proportional to the intensities of chorus waves. Actually the magnitude of local heating depends not only on the wave power available to heat the electrons but also on the number of electrons available to be accelerated, which is related to the electron distribution function. Incorporating this physical aspect into the current model is beyond the scope of the work to be presented here.

[36] To study the main physical processes in the inner magnetosphere, we made some assumptions. Although these assumptions can lead to uncertainties (for example, during the storm main phase the state of no internal source could also be a compromise of the added internal source and enhanced losses), the model results can quite well capture the time features in the PSD data decreases and increases. Therefore, the good simulation results for the individual storms with very high PE (Figures 2 and 4 and Tables 2–5) self-justified the forms of wave loss and heating terms used in our model.

[37] On the basis of the long-term study for the second half of 2002 and the detailed study of four storm events we see that the relative contribution of the two acceleration mechanism for outer radiation belt electrons, radial diffusion and internal heating, differs from storm to storm (also can be seen from the variations of the free parameters in each loss and heating term). It can be explained from the complicated nature of the wave-particle interactions, which besides the wave intensities depends on many factors such as particle energy and pitch angle, the ratio f_{pe}/f_{ce}, the spectral distribution of the wave power, the distribution of wave normal angles, the plasma composition and local time content. From this sense, even a full-dimensional diffusion codes equipped with parameterized diffusion coefficients may not be able to accurately simulate every storm. Instead, detailed information about above factors is needed and obviously this is beyond our current observation capabilities, and therefore the scope of this paper.

[38] Our model, though with some simplified assumptions, has its merit. First, instead of using a lumped electron lifetime we tried to approximate the expected losses of electrons from three different wave populations that interact with the electrons in different regions. Second, local heating is included in our model by adding an internal source term to the radial diffusion equation.

5. Conclusions

[39] In this report we combined newly available PSD data and our newly developed radial diffusion model to study the acceleration of relativistic electrons in the outer radiation belt. In our model, we parameterized the loss term by the different wave-particle interactions dominant in different L^* regions. We added an internal source as a function of the AE index to the radial diffusion equation to represent local heating.

[40] We considered PSD data at given μ and K, corresponding to 2.7 MeV electrons at $L^* = 4$ mirroring near the Earth's equator. The model results for the long-term run from 15 July 2002 to 31 December 2002 reproduced the average variations of radiation belt electrons between $L^* = 2.5$ and $L^* = 6$ but with overprediction and underprediction at different times, suggesting that the same set of parameters cannot be applied to all twelve storms in the second half of 2002. After detailed study of four individual storms, we found that three storms could be reproduced either by radial diffusion only with losses or by internal heating only with losses, but including both led to the best results; while the other storm clearly required significant local heating during the storm recovery phase.

[41] On the basis of our model results, we conclude the required magnitudes of radial diffusion and internal heating and the relative contributions of these two acceleration mechanisms responsible for the enhancement of energetic electrons in the outer radiation belt vary from storm to

storm. However, the reason for these differences needs further study. After comparing the results from different runs for four storms and analyzing the radial diffusion coefficients, we suggest that internal heating contributes more to the enhancements of the fairly high-energy electrons at $L^* = 4$. On the basis of our current results, it will be interesting to model the PSD variations corresponding to a much lower μ and to investigate how the relative contributions from radial diffusion and internal heating will change. This will be done in the future.

[42] **Acknowledgments.** This work was mainly supported by National Science Foundation grants.

[43] Zuyin Pu thanks T. Paul O'Brien and another reviewer for their assistance in evaluating this paper.

References

Abel, B., and R. M. Thorne (1998), Electron scattering loss in Earth's inner magnetosphere: 1. Dominant physical processes, *J. Geophys. Res.*, *103*(A2), 2385–2396, doi:10.1029/97JA02919.

Albert, J. M. (2003), Evaluation of quasi-linear diffusion coefficients for EMIC waves in a multispecies plasma, *J. Geophys. Res.*, *108*(A6), 1249, doi:10.1029/2002JA009792.

Baker, D. N. (2001), Satellite anomalies due to space storms, in *Space Storms and Space Weather Hazards*, *NATO Sci. Ser. 2*, vol. 38, edited by I. A. Daglis, pp. 285–311, Klouwer Acad., Dordrecht, Netherlands.

Baker, D. N., and S. Kanekal (2008), Solar cycle changes, geomagnetic variations, and energetic particle properties in the inner magnetosphere, *J. Atmos. Sol. Terr. Phys.*, *70*(2–4), 195–206, doi:10.1016/j.jastp.2007.08.031.

Baker, D. N., J. H. Allen, S. G. Kanekal, and G. D. Reeves (1998), Disturbed space environment may have been related to pager satellite failure, *Eos Trans. AGU*, *79*(40), 477, doi:10.1029/98EO00359.

Barker, A. B., X. Li, and R. S. Selesnick (2005), Modeling the radiation belt electrons with radial diffusion driven by the solar wind, *Space Weather*, *3*(10), S10003, doi:10.1029/2004SW000118.

Brautigam, D. H., and J. M. Albert (2000), Radial diffusion analysis of outer radiation belt electrons during the 9 October, 1990, magnetic storm, *J. Geophys. Res.*, *105*(A1), 291–309, doi:10.1029/1999JA900344.

Chen, Y., R. H. W. Friedel, and G. D. Reeves (2006), Phase space density distributions of energetic electrons in the outer radiation belt during two Geospace Environment Modeling Inner Magnetosphere/Storms selected storms, *J. Geophys. Res.*, *111*, A11S04, doi:10.1029/2006JA011703.

Chen, Y., G. D. Reeves, and R. H. W. Friedel (2007), The energization of relativistic electrons in the outer Van Allen radiation belt, *Nat. Phys.*, *3*(9), 614–617, doi:10.1038/nphys655.

Engebretson, M. J., et al. (2008), Pc1–Pc2 waves and energetic particle precipitation during and after magnetic storms: Superposed epoch analysis and case studies, *J. Geophys. Res.*, *113*, A01211, doi:10.1029/2007JA012362.

Fälthammar, C. G. (1965), Effects of time-dependent electric fields on geomagnetically trapped radiation, *J. Geophys. Res.*, *70*(11), 2503–2516, doi:10.1029/JZ070i011p02503.

Fei, Y., A. A. Chan, S. R. Elkington, and M. J. Wiltberger (2006), Radial diffusion and MHD particle simulations of relativistic electron transport by ULF waves in the September 1998 storm, *J. Geophys. Res.*, *111*, A12209, doi:10.1029/2005JA011211.

Fennell, J. F., H. C. Koons, J. L. Roeder, and J. B. Blake (2001), Spacecraft charging: Observations and relationship to satellite anomalies, in *Proceedings of 7th Spacecraft Charging Technology Conference*, edited by R. A. Harris, *Eur. Space Agency Spec. Publ., ESA SP-476*, pp. 279–285.

Fok, M.-C., R. B. Horne, N. P. Meredith, and S. A. Glauert (2008), Radiation Belt Environment model: Application to space weather nowcasting, *J. Geophys. Res.*, *113*, A03S08, doi:10.1029/2007JA012558.

Fraser, B. J., and T. S. Nguyen (2001), Is the plasmapause a preferred source region of electromagnetic ion cyclotron waves in the magnetosphere?, *J. Atmos. Terr. Phys.*, *63*(11), 1225–1247, doi:10.1016/S1364-6826(00)00225-X.

Green, J. C., and M. G. Kivelson (2004), Relativistic electrons in the outer radiation belt: Differentiating between acceleration mechanisms, *J. Geophys. Res.*, *109*, A03213, doi:10.1029/2003JA010153.

Horne, R. B., and R. M. Thorne (1998), Potential waves for relativistic electron scattering and stochastic acceleration during magnetic storms, *Geophys. Res. Lett.*, *25*(15), 3011–3014, doi:10.1029/98GL01002.

Horne, R. B., et al. (2005a), Wave acceleration of electrons in the Van Allen radiation belts, *Nature*, *437*, 227–230, doi:10.1038/nature03939.

Horne, R. B., R. M. Thorne, S. A. Glauert, J. M. Albert, N. P. Meredith, and R. R. Anderson (2005b), Timescale for radiation belt electron acceleration by whistler mode chorus waves, *J. Geophys. Res.*, *110*, A03225, doi:10.1029/2004JA010811.

Iles, R. H. A., A. N. Fazakerley, A. D. Johnstone, N. P. Meredith, and P. Bühler (2002), The relativistic electron response in the outer radiation belt during magnetic storms, *Ann. Geophys.*, *20*, 957–965.

Iles, R. H. A., N. P. Meredith, A. N. Fazakerley, and R. B. Horne (2006), Phase space density analysis of the outer radiation belt energetic electron dynamics, *J. Geophys. Res.*, *111*, A03204, doi:10.1029/2005JA011206.

Kim, H.-J., and A. A. Chan (1997), Fully adiabatic changes in storm time relativistic electron fluxes, *J. Geophys. Res.*, *102*(A10), 22,107–22,116, doi:10.1029/97JA01814.

Kondrashov, D., Y. Shprits, M. Ghil, and R. Thorne (2007), A Kalman filter technique to estimate relativistic electron lifetimes in the outer radiation belt, *J. Geophys. Res.*, *112*, A10227, doi:10.1029/2007JA012583.

Li, W., Y. Y. Shprits, and R. M. Thorne (2007), Dynamic evolution of energetic outer zone electrons due to wave-particle interactions during storms, *J. Geophys. Res.*, *112*, A10220, doi:10.1029/2007JA012368.

Li, X., D. N. Baker, M. Temerin, T. E. Cayton, E. G. D. Reeves, R. A. Christensen, J. B. Blake, M. D. Looper, R. Nakamura, and S. G. Kanekal (1997), Multisatellite observations of the outer zone electron variation during the November 3–4, 1993, magnetic storm, *J. Geophys. Res.*, *102*(A7), 14,123–14,140, doi:10.1029/97JA01101.

Li, X., M. Temerin, D. N. Baker, G. D. Reeves, and D. Larson (2001), Quantitative prediction of radiation belt electrons at geostationary orbit based on solar wind measurements, *Geophys. Res. Lett.*, *28*(9), 1887–1890, doi:10.1029/2000GL012681.

Li, X., D. N. Baker, M. Temerin, G. Reeves, R. Friedel, and C. Shen (2005), Energetic electrons, 50 keV–6 MeV, at geosynchronous orbit: Their responses to solar wind variations, *Space Weather*, *3*, S04001, doi:10.1029/2004SW000105.

Loto'aniu, T. M., R. M. Thorne, B. J. Fraser, and D. Summers (2006), Estimating relativistic electron pitch angle scattering rates using properties of the electromagnetic ion cyclotron wave spectrum, *J. Geophys. Res.*, *111*, A04220, doi:10.1029/2005JA011452.

Meredith, N. P., R. B. Horne, R. H. A. Iles, R. M. Thorne, D. Heynderickx, and R. R. Anderson (2002), Outer zone relativistic electron acceleration associated with substorm-enhanced whistler mode chorus, *J. Geophys. Res.*, *107*(A7), 1144, doi:10.1029/2001JA900146.

Meredith, N. P., R. M. Thorne, R. B. Horne, D. Summers, B. J. Fraser, and R. R. Anderson (2003a), Statistical analysis of relativistic electron energies for cyclotron resonance with EMIC waves observed on CRRES, *J. Geophys. Res.*, *108*(A6), 1250, doi:10.1029/2002JA009700.

Meredith, N. P., R. B. Horne, R. M. Thorne, and R. R. Anderson (2003b), Favored regions for chorus-driven electron acceleration to relativistic energies in the Earth's outer radiation belt, *Geophys. Res. Lett.*, *30*(16), 1871, doi:10.1029/2003GL017698.

Meredith, N. P., M. Cain, R. B. Horne, R. M. Thorne, D. Summers, and R. R. Anderson (2003c), Evidence for chorus-driven electron acceleration to relativistic energies from a survey of geomagnetically disturbed periods, *J. Geophys. Res.*, *108*(A6), 1248, doi:10.1029/2002JA009764.

Meredith, N. P., R. B. Horne, R. M. Thorne, D. Summers, and R. R. Anderson (2004), Substorm dependence of plasmaspheric hiss, *J. Geophys. Res.*, *109*, A06209, doi:10.1029/2004JA010387.

Meredith, N. P., R. B. Horne, S. A. Glauert, R. M. Thorne, D. Summers, J. M. Albert, and R. R. Anderson (2006), Energetic outer zone electron loss timescales during low geomagnetic activity, *J. Geophys. Res.*, *111*, A05212, doi:10.1029/2005JA011516.

Meredith, N. P., R. B. Horne, S. A. Glauert, and R. R. Anderson (2007), Slot region electron loss timescales due to plasmaspheric hiss and lightning-generated whistlers, *J. Geophys. Res.*, *112*, A08214, doi:10.1029/2007JA012413.

O'Brien, T. P., and M. B. Moldwin (2003), Empirical plasmapause models from magnetic indices, *Geophys. Res. Lett.*, *30*(4), 1152, doi:10.1029/2002GL016007.

O'Brien, T. P., M. D. Looper, and J. B. Blake (2004), Quantification of relativistic electron microburst losses during the GEM storms, *Geophys. Res. Lett.*, *31*, L04802, doi:10.1029/2003GL018621.

Reeves, G. D., R. H. W. Friedel, R. D. Belian, M. M. Meier, M. G. Henderson, T. Onsager, H. J. Singer, D. N. Baker, X. Li, and J. B. Blake (1998), The relativistic electron response at geosynchronous orbit during the January 1997 magnetic storm, *J. Geophys. Res.*, *103*(A8), 17,559–17,570, doi:10.1029/97JA03236.

Roederer, J. G. (1970), *Dynamics of Geomagnetically Trapped Radiation*, Springer, New York.

Schulz, M., and L. Lanzerotti (1974), *Particle Diffusion in the Radiation Belts*, Springer, New York.

Selesnick, R. S. (2006), Source and loss rates of radiation belt relativistic electrons during magnetic storms, *J. Geophys. Res.*, *111*, A04210, doi:10.1029/2005JA011473.

Selesnick, R. S., and J. B. Blake (2000), On the source location of radiation belt relativistic electrons, *J. Geophys. Res.*, *105*(A2), 2607–2624, doi:10.1029/1999JA900445.

Shprits, Y. Y., R. M. Thorne, G. D. Reeves, and R. Friedel (2005), Radial diffusion modeling with empirical lifetimes: Comparison with CRRES observations, *Ann. Geophys.*, *23*, 1467–1471.

Shprits, Y. Y., R. M. Thorne, R. Friedel, G. D. Reeves, J. Fennell, D. N. Baker, and S. G. Kanekal (2006), Outward radial diffusion driven by losses at magnetopause, *J. Geophys. Res.*, *111*, A11214, doi:10.1029/2006JA011657.

Shprits, Y. Y., N. P. Meredith, and R. M. Thorne (2007), Parameterization of radiation belt electron loss timescales due to interactions with chorus waves, *Geophys. Res. Lett.*, *34*, L11110, doi:10.1029/2006GL029050.

Summers, D., and R. M. Thorne (2003), Relativistic electron pitch-angle scattering by electromagnetic ion cyclotron waves during geomagnetic storms, *J. Geophys. Res.*, *108*(A4), 1143, doi:10.1029/2002JA009489.

Summers, D., R. M. Thorne, and F. Xiao (1998), Relativistic theory of wave-particle resonant diffusion with application to electron acceleration in the magnetosphere, *J. Geophys. Res.*, *103*(A9), 20,487–20,500.

Summers, D., B. Ni, and N. P. Meredith (2007), Timescales for radiation belt electron acceleration and loss due to resonant wave-particle interactions: 2. Evaluation for VLF chorus, ELF hiss, and electromagnetic ion cyclotron waves, *J. Geophys. Res.*, *112*, A04207, doi:10.1029/2006JA011993.

Thorne, R. M., T. P. O'Brien, Y. Y. Shprits, D. Summers, and R. B. Horne (2005), Timescale for MeV electron microburst loss during geomagnetic storms, *J. Geophys. Res.*, *110*, A09202, doi:10.1029/2004JA010882.

Turner, D., and X. Li (2008), Quantitative forecast of relativistic electron flux at geosynchronous orbit based on low-energy electron flux, *Space Weather*, *6*, S05005, doi:10.1029/2007SW000354.

Varotsou, A., D. Boscher, S. Bourdarie, R. B. Horne, S. A. Glauert, and N. P. Meredith (2005), Simulation of the outer radiation belt electrons near geosynchronous orbit including both radial diffusion and resonant interaction with Whistler-mode chorus waves, *Geophys. Res. Lett.*, *32*, L19106, doi:10.1029/2005GL023282.

Y. Chen and G. D. Reeves, Los Alamos National Laboratory, P.O. Box 1663, MS D466, Los Alamos, NM 87545, USA.

X. Li and W. Tu, Laboratory for Atmospheric and Space Physics, University of Colorado, 1234 Innovation Drive, Boulder, CO 80303, USA. (weichao.tu@colorado.edu)

M. Temerin, 1062 Woodside Road, Berkeley, CA 94720, USA.